Lawrence Berkeley National Laboratory

Title
EFFECT OF COMBUSTOR INLET GEOMETRY ON ACOUSTIC SIGNATURE AND FLOW FIELD BEHAVIOUR OF THE LOW SWIRL INJECTOR

Permalink
https://escholarship.org/uc/item/8bz9s22p

Author
Therkelsen, Peter L.

Publication Date
2010-06-14

Peer reviewed

GT2010-23498

EFFECT OF COMBUSTOR INLET GEOMETRY ON ACOUSTIC SIGNATURE AND FLOW FIELD BEHAVIOUR OF THE LOW SWIRL INJECTOR

Peter L. Therkelsen, David Littlejohn, and Robert K. Cheng
Lawrence Berkeley National Laboratory
Berkeley, California, USA

J. Enrique Portillo and Scott M. Martin
Siemens Energy, Inc.
Orlando, Florida, USA

ABSTRACT

Low Swirl Injector (LSI) technology is a lean premixed combustion method that is being developed for fuel-flexible gas turbines. The objective of this study is to characterize the fuel effects and influences of combustor geometry on the LSI's overall acoustic signatures and flowfields. The experiments consist of 24 flames at atmospheric condition with bulk flows ranging between 10 and 18 m/s. The flames burn CH_4 (at $\phi =$ 0.6 & 0.7) and a blend of 90% H_2 – 10% CH_4 by volume (at $\phi =$ 0.35 & 0.4). Two combustor configurations are used, consisting of a cylindrical chamber with and without a divergent quarl at the dump plane. The data consist of pressure spectral distributions at five positions within the system and 2D flowfield information measured by Particle Imaging Velocimetry (PIV). The results show that acoustic oscillations increase with U_0 and ϕ. However, the levels in the 90% H_2 flames are significantly higher than in the CH_4 flames. For both fuels, the use of the quarl reduces the fluctuating pressures in the combustion chamber by up to a factor of 7. The PIV results suggest this to be a consequence of the quarl restricting the formation of large vortices in the outer shear layer. A Generalized Instability Model (GIM) was applied to analyze the acoustic response of baseline flames for each of the two fuels. The measured frequencies and the stability trends for these two cases are predicted and the triggered acoustic mode shapes identified [Keywords: DLN, flame instabilities, acoustic model]

INTRODUCTION

To satisfy increasingly strict emissions regulations, modern gas turbine engines primarily operate by burning Lean Premixed (LP) natural gas. However, all LP turbine combustors experience undesirable dynamics under some conditions. Compared to diffusion flame burners, LP combustor dynamics are more complex due to unstable heat release which creates flow field instabilities and pressure oscillations [1].

Unsteady heat release in LP flames is caused by two mechanisms: fuel/air ratio oscillations and vortex shedding [2]. Fuel/air ratio oscillations are generated by acoustic oscillations in the premixing section, causing fluctuations in local mixedness of the fuel/air mixture. Combustion instabilities caused by fuel/air ratio oscillation most often occur near the lean blow out limit for a fuel, where small changes in fuel concentration can result in local pockets of noncombustible mixture. Conversely, vortex shedding is generated by flow separation primarily due to rapidly expanding combustor geometries, such as step changes in flow boundary at the dump plane of the injector into the combustion chamber. The large vortex structures are characterized by intense turbulence and shear stresses that distort the LP flame fronts and alter heat release rate. Removal of large-scale vortices and reduction of flow separation, by modifying combustor geometry with the addition of a quarl, has been shown to reduce pressure oscillations [3].

Specific design requirements of the LP combustion systems can limit the number of available options to control combustion dynamics. Unlike diffusion flame based combustors, LP systems operate at lower peak combustion temperatures and do not require large amounts of secondary air. Consequently, there are far fewer secondary air holes in the LP combustor liner to serve as acoustic dampers. Thus, the unsteady heat release of the LP flame, coupled with a lack of dampers in the combustor chamber, can turn the combustor into a resonating chamber [4]. In turn, the resonance can propel acoustic waves back to fuel injection sites leading to further fuel/air ratio fluctuations and flame instabilities. This feedback results in self-sustained, large amplitude, low frequency pressure oscillations [5]. If the magnitude of the pressure oscillations is sufficiently high, harmful effects can arise. These effects can include: non uniform exhaust gas thermal distribution, poor combustion

efficiency, thermal NO_x growth, and wall stress which can lead to premature hardware fatigue and failure [1].

While most LP gas turbines operate with natural gas fuel, interest in hydrogen-based syngas fuel derived from gasification of coal and biomass has grown in recent years. Studies show that a stable flame can become unstable (and vice versa) with the addition of hydrogen in the fuel stream [6, 7]. The cause of flame transition to a stable or unstable condition due to hydrogen fuel addition is linked to the change in the turbulent flame speed. As hydrogen concentration is increased in a LP flame, its turbulent flame speed also increases, due to the high reactivity of hydrogen. This turbulent flame speed change results in an increase in the bulk heat release rate and a shift in the axial location of the flame. If the location of heat release comes into phase with the combustor acoustic modes, large acoustic oscillations will develop [2].

OBJECTIVE AND BACKGROUND

The goal of this study is to gain some preliminary insights into the oscillation characteristics of the flame generated by the Low Swirl Injector (LSI). The LSI is a promising new technology for fuel-flexible LP gas turbines. It operates on a principle that is fundamentally different than those of other LP gas turbine injection systems. Traditional LP gas injection systems rely either upon bluff body or aerodynamic recirculation zone to stabilize the flame. In contrast, the LSI operates on a non-recirculating flame stabilization concept that exploits the propagating nature of lean premixed turbulent flames. Originally developed for laboratory fundamental studies [8-12], the LSI has been successful adapted to a range of ultra-low emission combustion applications. These applications include industrial heaters and natural gas fueled medium size gas turbines, achieving NO_x emission levels less than 5 ppm @ 15 % O_2 [13, 14]. In addition to the development for natural gas applications, the LSI has also been evaluated with fuels of a wide range of Wobbe indices to demonstrate its fuel-flexible capability [15, 16].

Although acoustic measurements of the LSI were not taken during the gas turbine tests or the laboratory high-pressure experiments, its combustion dynamics characteristics towards lean blow off were found to be different than those of the other LP combustors. Other than anecdotal evidence, the combustion oscillation characteristics of the LSI remain largely unexplored. In a study of the effect of acoustic forcing at various frequencies on flame heat release behavior of a small 2.54 cm diameter LSI, Kang et. al. [17] reported that thermoacoustic coupling of the flame with the acoustic forcing was mainly evident in the outer shear layer. In laboratory studies at atmospheric and high pressure conditions, with both methane and hydrogen based fuels, the outer shear layer, formed at the combustor entrance dump plane, is shown to influence flame stability, as well as the stabilization mechanism of the hydrogen flames [16]. These laboratory results show that the LSI is affected by the outer shear layer, and changing the inlet

geometry of the combustor can be a convenient and effective means to address some of the LSI flame oscillation characteristics.

In this study the effects of combustor entrance geometry on flame acoustics are analyzed to gain some insight to the oscillation characteristics of the LSI system. Two combustor geometries are considered. The first is a combustor with a 90° sudden expansion entry from the injector at the dump plane. The second has a divergent quarl of 30° half-angle at the entry to reduce corner vortex formation. The experiments include flames at atmospheric conditions burning CH_4 and a fuel mixture of 90% H_2 - 10% CH_4 at different equivalence ratios and bulk flow velocities. The diagnostics consist of pressure transducers, to characterize fluctuating pressure spectra, and Particle Image Velocimetry (PIV), to measure the turbulent flowfields. Additionally, a General Instability Model (GIM) has been developed and used to predict dominant acoustic frequencies generated by the LSI burner, as well as to conduct a first order stability analysis on the system. Since our current goal is to assess the validity of the GIM model and gain some insights for further development for future use as a predictive tool, a simplified combustor configuration without a restriction at the exit is chosen. Our next step is to develop a heat release model for the LSI flame in a combustor with exit restriction with and without a quarl at the entrance. When developed, the GIM can help explain changes in acoustic levels when different fuels, flow conditions, and combustor geometries used with the LSI burner. Additionally, the model will show what operating conditions and combustor geometries are less susceptible to self excited LSI flame oscillations.

NOMENCLATURE

D	LSI Diameter
GIM	General Instability Model
LP	Lean Premixed
LSI	Low Swirl Injector
P1 – P5	Pressure Transducers
PIV	Particle Image Velocimetry
$\overline{Q}$	Heat Release Rate
U_0	Bulk Flow Velocity
ϕ	Equivalence Ratio
r	Radial Distance
St	Struhal number
T_{ad}	Adiabatic Flame Temperature
x	Axial Distance

EXPERIMENTAL SETUP

The heart of the LSI is a shallow angle vane swirler surrounding an open center-channel that allows the center portion of reactants to remain un-swirled [9]. The non-swirling center flow inhibits vortex breakdown and promotes flow divergence, a key aerodynamic feature for the LSI flame stabilization method. The center channel is partially blocked
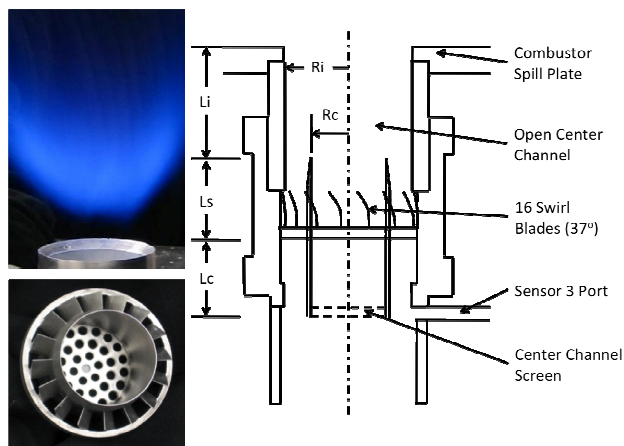
Figure 1 Schematic and photo of the LSI

with a screen to achieve the desired flow split between the center and outer swirling section. The LSI burner produces a lifted flame that stabilizes downstream of the injector exit plane (Figure 1). The distance between the injector exit plane and the flame is dependent upon the turbulent displacement flame speed of the fuel/air mixture and the divergence rate of the flow field generated by the LSI. The flame stabilizes at the point where the local displacement turbulent flame speed matches the local injector exit flow velocity.

The LSI used in this study is configured for NETL's SimVal high pressure experimental facility [16]. Key dimensions of this LSI are: Li = 6.8 cm, Lc = 2.2 cm, Ls = 2.8 cm, Ri = 2.8 cm, and Rc = 1.9 cm. The injector contains 16 aerodynamically shaped thickened blades with a 37° discharge angle. The center screen contains 37, 3.66 mm diameter holes arranged in a three concentric circle pattern surrounding a center hole. At SimVal, the center hole is reserved for pilot fuel injection that is needed for ignition only. Therefore, it was blocked for our experiments to simulate the LP configuration in SimVal. This center screen permits approximately 30% of the reactants to pass through the un-swirled center portion, with the remainder passing through the swirl vane annulus. This LSI has been developed specifically for experimental studies to support CFD validation. It has been optimized for fuel-flexible operation and can burn methane and pure hydrogen without requiring hardware change. Its design has been scaled to fit the sizes of other test facilities. The CAD model of the injector has been shared with many CFD developers.

In order to measure the acoustic signature of the LSI, an experimental test stand was constructed to facilitate pressure and PIV measurements. The schematic of the experimental flow system is shown in Figure 2. A venturi mixing tube premixes fuel and air before being fed into a cylindrical settling chamber. The LSI assembly is mounted on top of the settling chamber and contains a 5.6 cm diameter swirler. Mounted at the exit of the LSI, and on top of the combustor dump plane is a cylindrical chamber with dimensions identical to the combustor in NETL's SimVal high-pressure test rig [16]. The chamber is 18 cm in diameter and 32 cm tall, creating a 3.2:1 dump plane

to injector diameter ratio. For PIV measurements, a quartz tube is used as the combustion chamber. For acoustic measurements a stainless steel tube of the same dimensions with two pressure taps is used. The SimVal facility has an exit plate with an orifice opening of 9.0 cm. As discussed above, it was not used for this study to facilitate the acoustics analysis. To modify the dump plane geometry, a detachable quarl of 3.8 cm tall with 30° half angle is used. This short quarl doe not completely obscure the flame to allow PIV interrogations of the flame's trailing edge for gaining some insight on the quarl's effects on the flowfield. As shown by the images of Fig. 2, the leading edge of the flame resides inside the quarl. However, the flame position and the overall flame shape are relatively unaffected by the use of the quarl.

The experimental setup of Figure 2 is an atmospheric system supplied by a fan-blower. It supplies air between 0.16 and 1.05 kg/s, corresponding to LSI exit bulk flow velocities, U_0, from 3 to 20 m/s. Fuel flows are supplied through computer controlled mass flow controllers upstream of the mixing tube. Therefore, the reactants are assumed to be well-mixed and the observed oscillations cannot be caused by inlet fuel/air ratio fluctuations.

Acoustic dynamics of the combustor system were measured by attaching five sensors to the locations, P1 – P5, indicated in Figure 2. The first three are located in the air inlet line (P1), premixer plenum (P2), and just upstream of the swirler blades (P3). The two sensors mounted on the side arms of the combustion chamber are located at 3.8 cm from the combustor top (P5) and bottom (P4) respectively. For this our first investigation of flame acoustics, we elected to utilize economical and readily available pressure transducers to acquire the acoustic signals - Freescale Semiconductor MPX5010 differential pressure sensors with 10 kPa differential pressure range. The manufacturer specifies a 1 ms response for the transducer output to change from 10% to 90% of the final value in response to a step change in pressure. While the
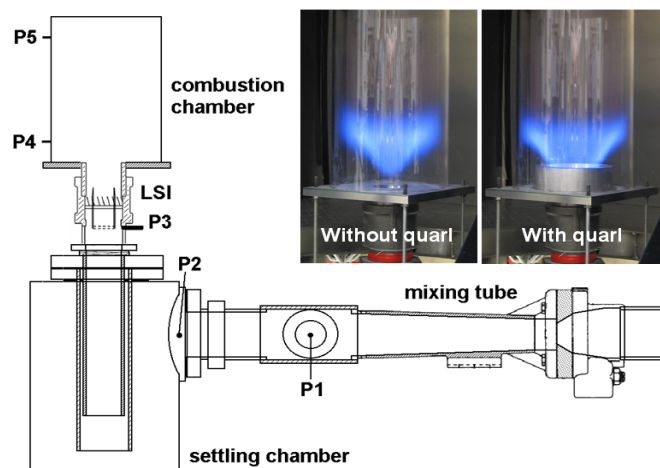

Figure 2 Schematic of the flow system for PIV and acoustic measurements

transducer's response to high frequencies will be attenuated, it should be adequate for a comparative study of the flame acoustics signatures with dominant frequencies at about 350 Hz as indicated by a preliminary microphone investigation. Additionally, comparison of the pressure transducer and microphone acoustics spectra showed that the Freescale transducers have significant responses up to 3500 Hz. This suggests that the manufacturer's specification is conservative. The pressure sensor signals were recorded using a National Instruments A/D board. Pressure data were sampled and recorded at 5000 Hz for 1.64 seconds from each of the five sensors located on the experiment (Figure 2). Fourier transforms of the signals were obtained to identify the frequencies of oscillations that occurred at tested operating conditions.

Axial location of heat release from the enclosed LSI flames was estimated with unfiltered flame luminescence. Images were recorded with a Xybion ICCD camera with a spectral sensitivity range of approximately 300 to 800 nm (UV response limited by lens cutoff). The luminescence images were processed to obtain a mean intensity profile along the flow axis to be used as inputs to the acoustic model. Measurements show the emissions from the 90% hydrogen flames were significantly closer to the injector outlet than those of the methane flames. This means an upstream shift in the H_2 flame position that is consistent with previous observations [16].

Details of the PIV system and data analysis are described in [13]. The system is based around a New Wave Solo PIV laser, with double 120 mJ pulses at 532 nm and a Kodak/Red Lake ES 4.0 digital camera with 2048 by 2048 pixel resolution. The optics are configured to capture a 13 cm by 13 cm field of view. A cyclone particle seeder seeds the airflow with Aerosil 200, synthetic amorphous silica particles, with nominal size of 12 nm. Data analysis was performed on 224 image pairs for each experiment, with software developed by Wernet [18]. Using 64 x 64 pixels cross-correlation interrogation regions with 50% overlap, a spatial resolution of approximately 2 mm is rendered.

EXPERIMENTAL RESULTS

The experiments were conducted with CH_4 and a 90% H_2 - 10% CH_4 fuel blend by volume. The 90% hydrogen fuel is used instead of pure hydrogen because the 90% H_2 fuel produces visible flames to allow for easy detection of burning in the outer shear layer, which occurs at high ϕ. Outer shear layer burning is due to a combination of the higher turbulence intensities in the shear layer and the increase in the displacement flame speed of H_2. As discussed in Cheng et. al. [16] the hydrogen based flame eventually attaches to the rim of the LSI and forms into a M-shaped flame when burning at typical gas turbine flame temperatures of 1700K < T_{ad} < 1800K. For the current LSI, the attachment limit of the 90% H_2 - 10% CH_4 flames was found to be at ϕ > 0.4. Consequently, the experiments with the 90% H_2 fuel had to be conducted below this limit to avoid the
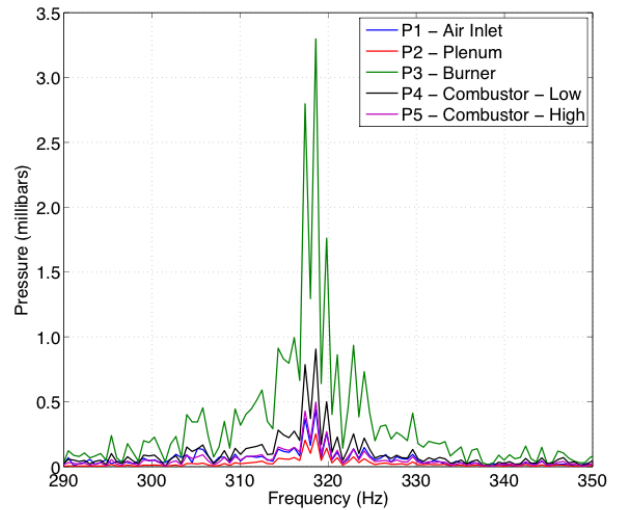

Figure 3 Spectral plot for CH_4 baseline case from all sensors

complications introduced by the changes in flame/flow interaction process associated with flame attachment.

The experiments were performed at U_0 = 10, 15, and 18 m/s with CH_4 at ϕ = 0.60 and 0.70, the 90% H_2 -10% CH_4 fuel at ϕ = 0.35 and 0.40. As such, the Adiabatic Flame Temperatures (T_{ad}) of the methane flames (1669K at ϕ = 0.6 and 1847K at ϕ = 0.7) are higher than those of the 90% H_2 - 10% CH_4 flames (1270K at ϕ = 0.35 and 1384K at ϕ = 0.4). The combustor without the quarl, i.e. sudden expansion dump plane at the entry is the baseline configuration. The two baseline flames are CH_4 at ϕ = 0.7 and 90% H_2 - 10% CH_4 at ϕ = 0.4, both at U_0 = 18 m/s. Though the flame temperatures of the two baseline cases are not matched, their volumetric heat release rates are similar to give a valid basis for the acoustics analysis.

Pressure spectral distribution from the five sensors, P1 – P5, obtained for the CH_4 baseline flame is seen in Figure 3. The plot indicates that the five sensors report the same frequency responses. The pressure spectral distributions of all sensors span across a large frequency range up to 2500 Hz. This figure focuses on a small frequency range that displayed significant responses. Data from P4, located 3.8 cm above the bottom of the combustion chamber, is exclusively presented throughout the rest of the paper. This sensor is of interest due to its location near the flame.

Peak frequency and fluctuating pressure at P4 for the eight CH_4 and 90% H_2 – 10% CH_4 flames at U_0 = 18 m/s are listed respectively in Tables 1 and 2. The two baseline cases are highlighted in bold face. From these Tables the effects of flow and combustor geometry changes can be evaluated. Starting with the two baseline cases, they both excited the same frequency of 320 Hz. The peak pressure magnitudes of the 90% H_2 – 10% CH_4 baseline flame is three times higher than the CH_4 baseline flame, even though the CH_4 flame releases 113 kW,
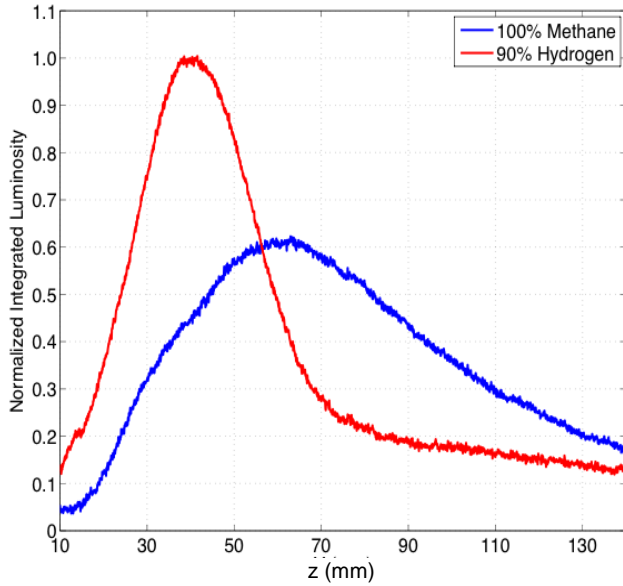
Figure 4 Mean heat release rate profiles measured in the two baseline cases

compared to 74 kW released by the 90% H_2 – 10% CH_4 flame. The difference in the fluctuating pressure magnitude is most likely associated with the different flame locations and the heat release distribution as seen in Figure 4. Due to the flames extending beyond the image area of the camera, quantified heat release values cannot be deduced for the baseline flames. Instead, integrated luminosity values in the radial direction, normalized to the peak value of the 90% H_2 – 10% CH_4 flame are plotted. Figure 4 shows the 90% H_2 -10% CH_4 flame is more compact as indicated by the narrower peak of its heat release rate profile. The flame brush is closer to the combustor entrance and releases the bulk of its energy at a higher rate than the methane flame. The heat release rate profiles are used in the GIM analysis and discussed below.

Table 1 Peak frequencies and fluctuating pressure at P4 for CH_4 flames at $U_o = 18$ m/s

	Peak Frequency (Hz)	Peak Fluctuating Pressure (millibars)	Normalized Peak Fluctuating Pressure
φ = 0.7 w/o Quarl	**319**	**0.90**	**1.00**
φ = 0.7 w/ Quarl	529	0.13	0.14
φ = 0.6 w/o Quarl	293	0.14	0.15
φ = 0.6 w/ Quarl	472	0.12	0.13

Table 2 Peak frequencies and fluctuating pressure at P4 for 90% H_2 - 10% CH_4 flames at $U_o = 18$ m/s

	Peak Frequency (Hz)	Peak Fluctuating Pressure (millibars)	Normalized Peak Fluctuating Pressure
φ = 0.4 w/o Quarl	**320**	**2.72**	**1.00**
φ = 0.4 w/ Quarl	500	0.39	0.14
φ = 0.35 w/o Quarl	406	0.82	0.30
φ = 0.35 w/ Quarl	408	0.11	0.04

As equivalence ratio and entrance geometry are varied, both peak frequency and pressure fluctuation magnitude shift. Though the shifting trends are not the same for the two fuels, the addition of a 30° quarl creates a consistent reduction in the peak fluctuating pressure. For CH_4 at φ = 0.7, peak fluctuating pressure is reduced to 14% of the baseline value, with the associated frequency increasing to 529 Hz. Interestingly, the quarl also reduced the peak fluctuating pressure of the 90% H_2 – 10% CH_4 φ = 0.4 flame by the same relative amount, to about 14% of the corresponding baseline value. Its peak frequency also shifted to 500 Hz.

In general, lowering φ for both fuels, i.e. lowering the total heat release, results in an overall reductions in the peak fluctuating pressure. For CH_4 without the quarl, changing φ from 0.7 to 0.6 lowers the peak fluctuating pressure to 15% of the baseline value, even though the change in total heat release is comparatively modest from 117 kW to 81 kW. Due to the relatively low peak fluctuating pressure of the CH_4 φ = 0.6 flame, the use of the quarl brings about a quantifiable but very small decrease. For the 90% H_2 – 10% CH_4 flames without the quarl, lowering φ from 0.4 to 0.35 reduces the peak fluctuating pressure to 30% of the baseline value. It is also interesting to note that the peak fluctuating pressure of the 54 kW, φ = 0.35, 90% H_2 – 10% CH_4 flame is about same as the baseline φ = 0.7 CH_4 flame which has more than two times the total heat release. This observation supports the notion that the higher local heat release rate of hydrogen flames may account for the high fluctuating pressures. With the quarl, the peak fluctuating pressure of the φ = 0.35, 90% H_2 – 10% CH_4 flame is reduced to about 13% of valued measured in the corresponding flame without the quarl.

In Figure 5, the effects of flow velocity on acoustics signatures are shown by the contours plots of fluctuating pressure on the frequency versus U_0 plane. Due to the large range in the peak fluctuating pressures, the contours are plotted with a nonlinear, 0-1 millibar, color scale to show details at the lower pressure levels. This scale covers variations in pressure for all cases except for some points of the 90% H_2 – 10% CH_4 flames which exceed 1 millbar. Note that there is a strong line seen in every case at 480 Hz, which is an artifact of the experimental system. This is confirmed by measuring the pressure spectra for cases with air only and with the reactants flowing into the LSI but without lighting the flame.

In general, the fluctuating pressures of the 90% H_2 – 10% CH_4 flames are higher than those of 100% CH_4 flames. As U_0 decreases, pressure levels across the whole frequency spectrum also decrease due primarily to the reduction in total heat release. However, the shifts in the peak frequencies with decreasing U_0 are not consistent. This is clearly seen in the cases with no quarl (left column). For the two methane sets at φ = 0.6 and 0.7 and also the set for 90% H_2 – 10% CH_4 at φ =

5

0.35, the peak pressure frequency decreases with decreasing U_0. In contrast, the set for 90% H_2 – 10% CH_4 at $\phi = 0.4$ shows an opposite trend with the peak pressure frequency increases with U_0.

Comparing the contours on the left column of Figure 5 (without quarl) to those on the right column (with quarl), it is clear that the quarl is effective in reducing the peak fluctuating pressure. During the experiments, the effectiveness of the quarl was readily observed as it lowered the audible flame noise quite significantly. However, the fluctuating pressure spectra and reduction in flame noise cannot fully explain how changes in fuel, flow, and combustor geometry alter the acoustic response of the system.

To gain further insights, PIV measurements were made to investigate the effect of the quarl on the reacting and non-reacting flowfields. 2D velocity vectors for the baseline cases with the contours of the Reynold stress plotted in the background are shown in Figure 6. The corresponding fluctuating pressure spectra obtained at P4 are shown to their left with the location of P4 indicated on the velocity vector plots. Because the quarl obscured the combustor entrance, the PIV field-of-view for these cases was moved 3.8 cm downstream to capture the flow exiting the quarl.

PIV measurements made inside the quartz cylinder are corrupted by the reflection of the incident laser light from the inner and outer surfaces. The defects are clearly seen as the bright vertical stripes on the raw PIV image (Figure 7). This causes data dropout due to an increase in signal to noise ratio. In the velocity vector plots, the laser reflection imprints generate vertical strips of high Reynolds stresses or data
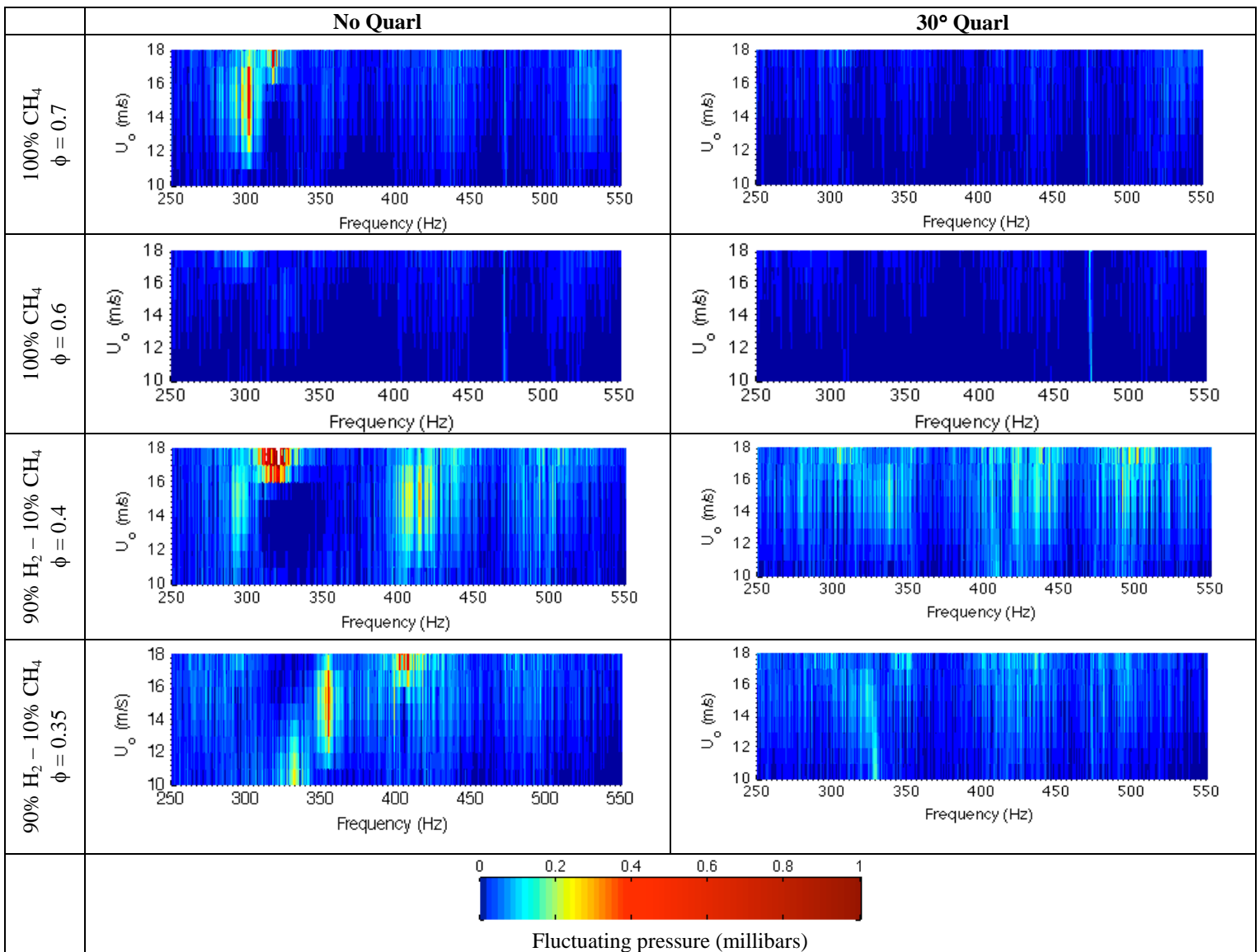

Figure 5 Contours of baseline cases and varied operational parameters

dropout at r/D = -0.5, -0.7, 0.7 and 1.

For the baseline cases without quarl shown in the top row of Figure 6, the Reynolds stress contours clearly outline the formation of a shear layer at the rim of the LSI. Flow tracing of the velocity vectors outside of the shear layer outlines a circular pattern to indicate the formation of a recirculation zone at the corner of the dump plane. Inspection of the raw PIV images (Figure 7) and also the instantaneous velocity vectors showed that the shear layer is characterized by large coherent rolled up vortex structures entraining combustion products trapped in the corner. These large structures, when convected downstream, interact with the trailing edge of the LSI flame. The most likely consequence of such interaction will be oscillations in heat release rate that may explain the strong pressure peaks seen for both fuels around 320 Hz. With the quarl, the vector plots in the bottom row of Figure 6 indicate that it guided the flow into a slightly more divergent pattern than the baseline cases. As seen in Fig. 2, use of the quarl does not change the overall flame shape and its mean positions. Consequently, except for the formation of a weak central recirculation zone in the farfield of the CH_4 flame, the quarl does not alter the overall flowfield features. The level of shear stresses at the exit of the quarl is comparatively lower than the baseline cases. Because the quarl fills the void at the corner of the dump plane, large vortex structures cannot be formed in the shear layer to affect the flame. The reduction in the fluctuating pressure is apparent by the lack of peaks at 320 Hz. Although there are other mechanisms that may have contributed to the LSI flame acoustics, the formation of the corner recirculation zone seems to be the leading cause of flame instability.

ACOUSTIC MODEL FOR BASELINE CASES

Results presented in this section are aimed at attaining a preliminary assessment of the thermoacoustic behavior of the LSI flame. It should be emphasized that the analysis presented here are intended as a first step towards developing a fundamental understanding of this flame in this particular system.

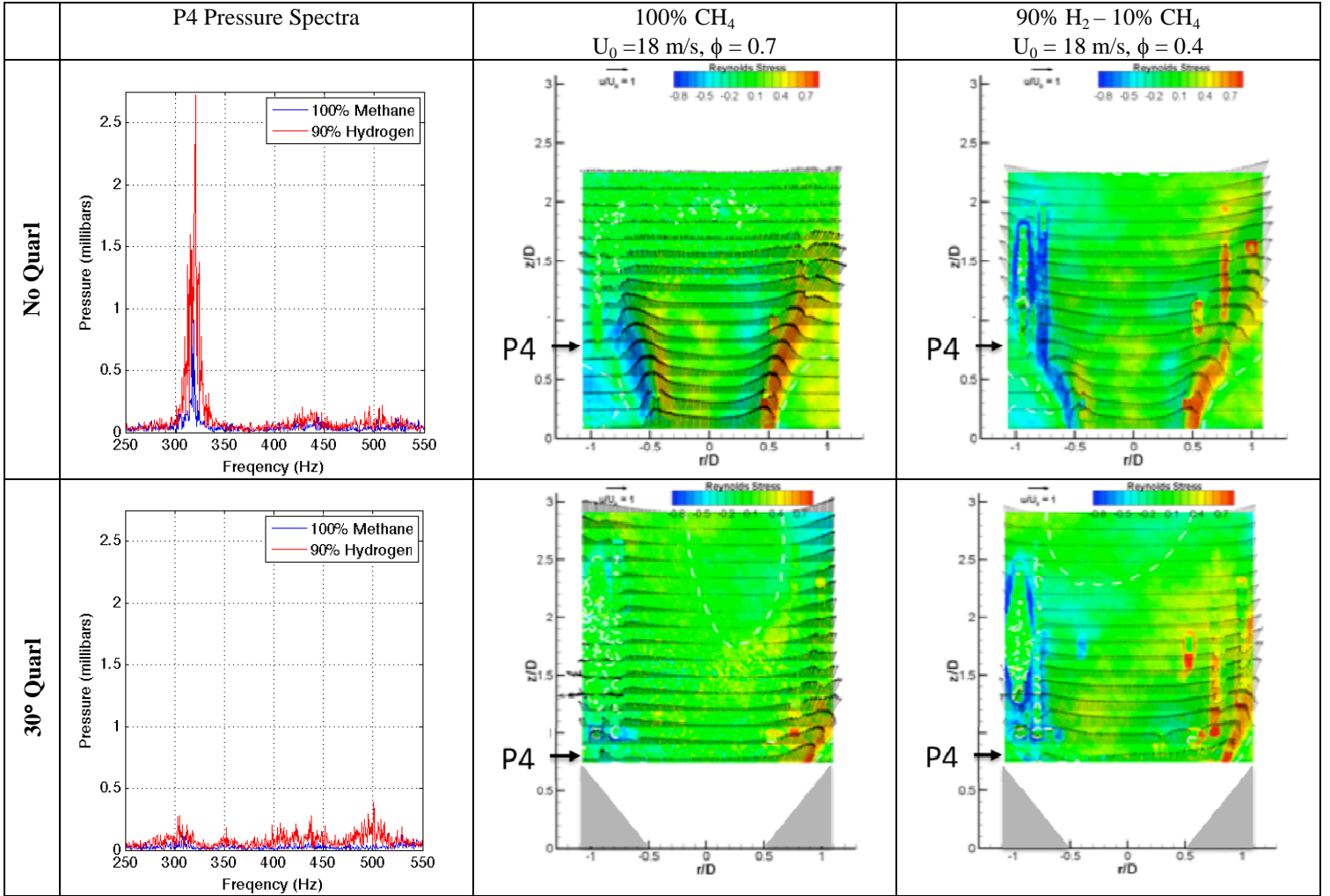|	P4 Pressure Spectra	100% CH$_4$ U$_0$ =18 m/s, ϕ = 0.7	90% H$_2$ – 10% CH$_4$ U$_0$ = 18 m/s, ϕ = 0.4
No Quarl			
30° Quarl			

Figure 6 Pressure spectral distributions and 2D mean velocity vectors obtained for the baseline cases with and without quarl

The experimental system shown schematically in Figure 2 is designed for atmospheric conditions and does not allow for choked points to isolate the acoustics boundaries. Therefore, an acoustic system with open boundaries would be the best approximation to model its acoustic features. Open boundary systems similar to the one being considered here have been modeled by a General Instability Model [19]. GIM solves the eigenfrequencies via a linearized Euler solver [20] and solves for the temporal stability of the system by solving a wave equation via the modified Galerkin method [21].

Figure 8 shows the schematic of acoustic model for the LSI and the combustion chamber as an open straight duct consisting of three zones. Zone 1, where P3 is located, is the supply pipe of the LSI that fits inside the plenum, and includes the swirler. Zone 2 is the combustor entry and Zone 3 is the combustor with a non-restricted open exit where P4 and P5 are installed. For this first preliminary study, GIM has been applied to the two baseline cases without quarl in order to *verify* its validity for the

LSI system. Implementation of GIM to the other geometries and flow conditions are outside the scope of this paper and are left for future work. Table 3 presents the flow properties at each zone. Note that only zone 3 is different between the two baseline cases due to the differences in their flame temperature.

Table 3 Flow properties for acoustic model

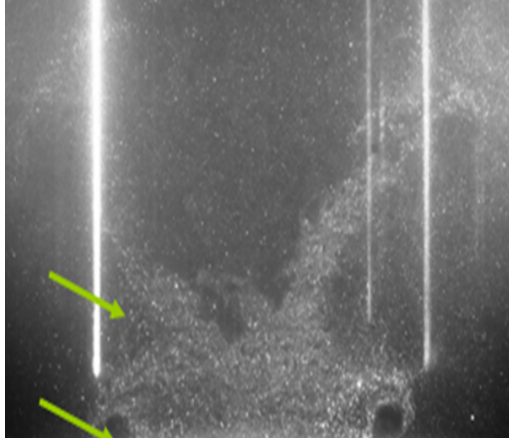|	units	Zone			
		1	2	3 (CH$_4$)	3 (H$_2$)
Length	m	0.45	0.04	0.28	0.28
Diameter	m	0.06	0.18	0.18	0.18
Temp.	°K	290	290	1837	1382
Press.	atm	1	1	1	1
Sonic Velocity	m/s	341	341	826	738
Density	Kg/m^3	1.2	1.2	0.19	0.24

Figure 8 Schematic of the acoustic model

Table 4 shows frequencies obtained for baselines CH$_4$ and 90% H$_2$ – 10% CH$_4$ flames with GIM's linear Euler solver. As can be seen, the predictions of the GIM first longitudinal (1L) mode compare very well with experimental data for both flames. The small peak observed near ~500 Hz, as seen in Figure 6, corresponds to the 2L. However, the signal strength is too low to provide a single frequency with confidence. A computed 3L frequency of ~780 Hz, which differs from the small peaks observed ~650 Hz, suggests the ~650 Hz is a harmonic of the 1L mode or that the plenum and premixing tube may be participating at these higher frequencies.

The normalized acoustic pressure for the 1L and 2L modes of the CH$_4$ baseline case are plotted in Figure 9 alongside the normalized maxima of the measurements made at locations P3, P4 and P5 for both CH$_4$ and 90% H$_2$ - 10% CH$_4$ cases. Not shown here are the mode shapes for the 90% H$_2$ - 10% CH$_4$ case; this is because the mode shape does not vary significantly between the two baseline cases. In this figure, an axial position of zero corresponds to the entrance to the inlet pipe. The swirler is located at 0.34 m from the entrance and the dump plane at 0.45 m. No measurements are included for the 2L mode due to the small acoustic pressure amplitudes observed at these frequencies (see Figure 6).

The 1L has a pressure anti-node very close to the location of the swirler (P3 is located slightly upstream of the swirler entrance) while the 2L has a pressure node at this location. Note how the normalized measurements follow closely the trend for the 1L mode. Given the good match between measurements and calculations in both frequency and mode shape, it is concluded that the triggered mode in this system corresponds to the first longitudinal acoustic mode of the open-open system.

Table 4 Measured and predicted acoustic frequencies and Strouhal numbers for the baseline flames highlighted in bold type in Tables 1 and 2

Case	mode	Measurements		GIM	
		Freq (Hz)	St	Freq. (Hz)	St
CH$_4$	1L	319	13.6	323	13.8
	2L	-	-	483	20.7
	3L	-	-	783	33.5
90% H$_2$ - 10% CH$_4$	1L	320	13.7	320	13.7
	2L	-	-	472	20.2
	3L	-	-	779	33.3

Next, GIM was used to perform a stability analysis of the system. To represent the flame in the analysis, a distributed heat addition n-τ model is used:

$$q'(x,t)/\overline{q}(x) = n \cdot p'(x,t-\tau)/\overline{p}$$

and:

$$\overline{q}(x) = \frac{\overline{Q}}{A}\left(\frac{1}{\sigma\sqrt{2\pi}}e^{-\left(\frac{(x-\mu)^2}{2\sigma^2}\right)}\right)$$

where n represents the interaction index of the model, τ the time lag between pressure and the heat addition, $\overline{Q}$ is the heat release rate, A the cross sectional area, σ and μ the normal distribution's mean and standard deviation [22].

This model assumes that the strength of the flame oscillations is proportional to the measured, distributed heat release rate, and that the perturbations are in phase with local acoustic pressure fluctuations (by setting τ to zero). It should be noted that this model *does not* represent a specific mechanism per se; it only mimics the location and strength of the forcing that the flame unsteadiness provides to the system, independently of the mechanism that caused the unsteadiness.

To simplify the analysis, the heat release distribution measured from the luminescence images (see Figure 4) is approximated by a Gaussian distribution and applied to the model. Figure 10 shows the axial distribution for the two baseline cases implemented into GIM.

GIM stability analysis of the system for the first longitudinal mode results in linear growth rates as tabulated in Table 5. In this model, positive values of growth rates correspond to linearly unstable cases. The assumption of zero time delay between the local acoustic pressure field and the local heat release rate means that the flame responds instantly to local pressure perturbations. Although this assumption precludes other mechanisms that may have contributed to the flame/acoustics coupling, this provides a starting point as a first effort to understand the acoustic response of the LSI, and helps to establish initial hypothesis that will direct future tests and as well as model development.
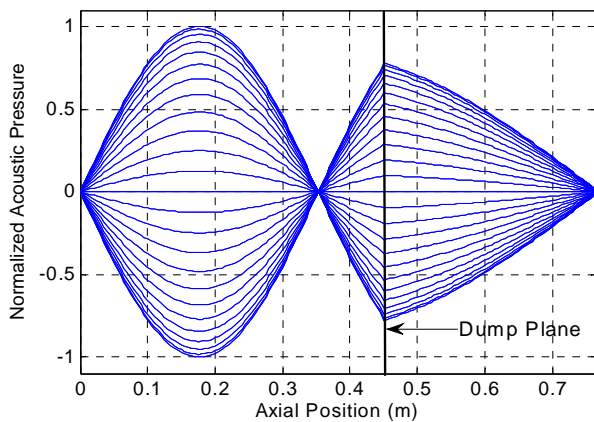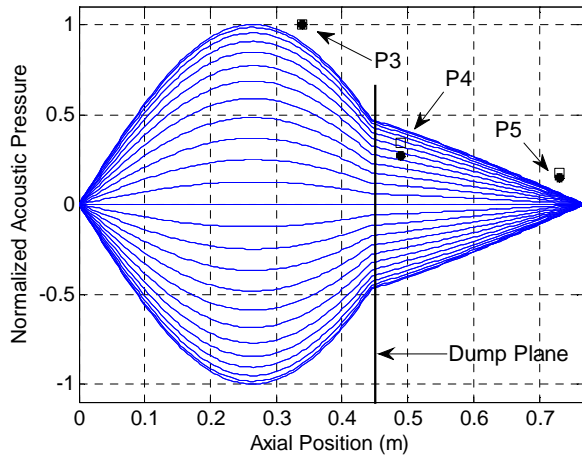
Figure 9 Computed first (top) and second (bottom) longitudinal mode shapes for the baseline CH_4 case. Data points are from experiments with closed circles correspond to CH_4 and open squares to 90% H_2 - 10% CH_4.

Table 5 Calculated growth rates for baseline cases

Case	mode	μ	σ	Q_{vol}	Growth Rate
		m	m	MW/m3	rad/sec
CH_4	1L	0.53	0.024	74.1	2.71
90% H_2 10% CH_4	1L	0.50	0.015	77.1	3.02

For the 1L mode, these calculations show a larger growth rate for the 90% H_2 - 10% CH_4 case than for the CH_4 flame. This is in agreement with the measurements. Physically, three effects are taking place as H_2 fuel is added and the equivalence ratio is lowered:

(1) The flame moves upstream due to the increased flame speed. This increases the system instability since the flame sits closer to the pressure anti-node.
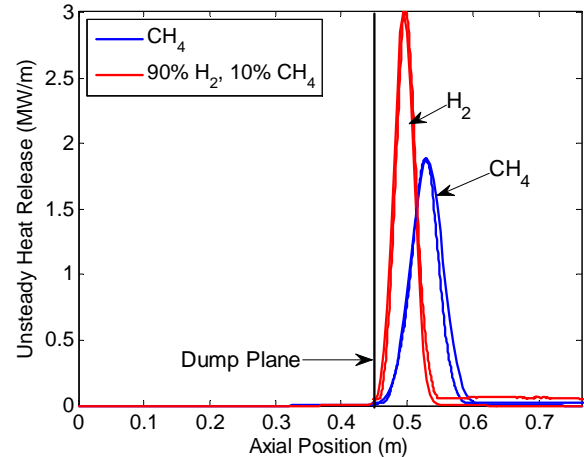

Figure 10 Distributed unsteady heat release rate for baseline cases. The dashed lines are taken from Figure 4.

(2) The flame brush becomes thinner due to increased reactivity of H_2. This increases the energy density of the perturbations and thus, the instability level.
(3) The combustion energy decreases due to the lower flame temperature. This decreases the energy input and therefore the strength of the oscillations.

A combined effect of the last two points is reflected in the heat release per unit volume (see Q_{vol} in Table 5). As it can be seen, they are very close to each other, meaning that both cases are forced with the same relative energy despite a significant difference in the total energy. Additionally, since the two baseline cases have the same Strouhal number (see Table 4), changes in macroscopic convective processes are not a factor here. Therefore, in can be postulated that the 90% H_2 - 10% CH_4 case is more unstable than the CH_4 case mostly because the flame is moved upstream, closer to the 1L pressure anti-node.

Since the 2L mode is not triggered by the system and the unsteady heat release model selected here does not model any particular mechanism, a stability analysis for the 2L mode will not represent any flow physics and is therefore not pursued.

Insight as to why the 2L mode is not triggered can be gained by analyzing the perturbation velocity mode shape as shown in Figure 11. For clarity, this figure shows only the envelope of the velocity fluctuations as a function of the axial location. As it can be seen, a velocity node is present at the dump plane for the 2L mode; this indicates that velocity perturbations near the corner recirculation zone are smaller than for the 1L case, for which velocity fluctuations are not as small. This supports the hypothesis that the corner recirculation zone is one of the mechanisms responsible for LSI instabilities.

Finally, it is worthwhile to note that in order to model the instability mechanisms, models such as those in which the unsteady heat release is coupled to velocity or mass flow rate perturbations, with their corresponding time delay, need to be used. As mentioned previously, these studies are outside of the scope of this paper and are therefore left as future work.

DISCUSSION

The velocity data and visual evidence shown on the PIV raw images indicate that the coherent vortex rings shed from the dump plane are most likely responsible for triggering the self-excited flame instability observed in the baseline cases. A significant finding is of course the fact that the addition of the quarl resulted in much more stable operation. This is most likely due to a decrease in the magnitude of the local radial velocity gradients in the shear region. Smaller velocity gradients indicate a less unstable system.

The pressure spectral distributions measured in this system also raised may questions such as:

1. What are the mechanisms that control the peak frequencies and their shifting trends with U_0 and ϕ ?
2. What can be learned from the frequency shift regarding the flame/chamber interactions?
3. How to utilize the observed pressure oscillations to help address combustion dynamics problems?

Although the GIM is a lower order model for the combustion oscillations, its application to the LSI system has helped to identify the main cause of the self-excited acoustic instabilities. We plan to continue the development of the GIM model to consider the variation in the combustor geometry such as the quarl configuration and the restriction at the combustor exit. Unsteady heat release models for the LSI will also be developed. As to the experiments, the analysis also indicates that simple changes in the dimensions of the experiments can bring about fresh insights on the acoustic properties of the LSI flames. These include varying the positions of the node points by changing the length and diameter of the combustion chamber and also the length of the LSI feed pipe. Our approach is to conduct a coordinated experimental and modeling effort to understand the mechanisms causing instabilities in enclosed LSI
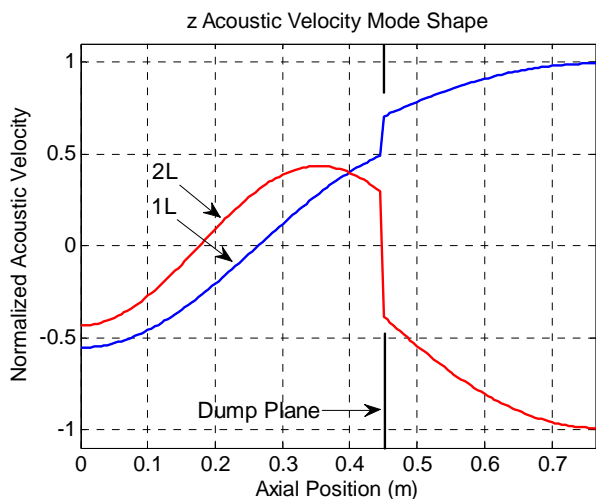

Figure 11 Computed first and second longitudinal velocity mode shape for the baseline CH_4 case.

flames and to develop combustor geometries that minimize the acoustic coupling with the LSI flame.

CONCLUSIONS

The fuel effects and influences of combustor geometry on flame acoustics have been studied and analyzed to gain some insight into the oscillation characteristics of the LSI system. The experimental LSI is developed to support CFD research and is capable of burning CH_4 and H_2 flames without requiring hardware change. Two combustor geometries are considered in this study. The first is an open end cylindrical chamber with a 90° sudden expansion entry and the second is the same open-ended combustor fitted with a divergent quarl of 30° half-angle at the entry. The experiments include flames at atmospheric conditions burning CH_4 and a fuel mixture of 90% H_2 - 10% CH_4 at different equivalence ratios and bulk flow velocities form 10 to 18 m/s. The diagnostics consist of dynamic pressure transducers to characterize fluctuating pressure spectra and Particle Image Velocimetry (PIV) to measure the turbulent flowfields.

The pressure spectral distribution show that all flame excites acoustics frequencies between 300 to 400 Hz with the highest pressure fluctuating intensities at 320 Hz corresponding to the first longitudinal resonance frequency of the assembly consisting of the LSI supply tube and the combustion chamber. As expected, the acoustic oscillation level increase with U_0 and ϕ due to the increases in the bulk heat release rates of the flames. The fluctuating pressures measured in the 90% H_2 - 10% CH_4 flames are significantly higher than in the CH_4 despite the fact that the bulk heat release rates of the 90% H_2 - 10% CH_4 flames are lower. Comparison of the mean heat release profiles along the axis of the combustor show that the 90% H_2 - 10% CH_4 flame has a higher local release rate due to a narrower flame brush. The flame positions also shift closer to the dump plane due to an increase in the turbulent flame speed compared to the CH_4 flame.

For both fuels, the use of the quarl reduces the fluctuating pressures in the combustion chamber by up to a factor of 7. The PIV results show this to be a consequence of the quarl restricting the formation of large vortices in the outer shear layer. Without the quarl, the 2D velocity vectors outline a recirculation zone formed at the corner of the combustor dump plane. From the raw PIV Mie scattering image, the shear layer is characterized by coherent vortex rings shedding from the LSI lip to trigger self-excited flame instabilities. With the quarl, the overall flowfield features are not significantly altered except for the fact that the shear stresses in the shear layer are lowered.

A General Instability Model (GIM) has been applied to predict dominant acoustic frequencies generated by the LSI and to conduct a stability analysis on two baseline flames without the quarl. The results show that GIM is able to model the self-excited combustion instabilities and confirms that the LSI triggers the 1L mode of the system. The analysis also suggests that the higher instabilities observed in the baseline 90% H_2 -

10% CH$_4$ is attributed to the flame moving upstream with respect to the baseline CH$_4$ flame. The implication is that the source of unsteady heat release has moved closer to a pressure anti-node and therefore increases the system instability.

ACKNOWLEDGMENTS

REFERENCES

[1] Lieuwen, T. C., 2003, "Statistical Characteristics of Pressure Oscillations in a Premixed Combustor," Journal of Sound and Vibration, 260(1), pp. 3-17.

[2] Lieuwen, T., Mcdonell, V., Petersen, E., and Santavicca, D., 2006, "Fuel Flexibility Influences on Premixed Combustor Blowout, Flashback, Autoignition and Stability," ASME Turbo Expo 2006: Power for Land, Sea and Air, GT2006-90770.

[3] Syred, N., 2006, "A Review of Oscillation Mechanisms and the Role of the Precessing Vortex Core (Pvc) in Swirl Combustion Systems," Progress in Energy and Combustion Science, 32(2), pp. 93-161.

[4] Fichera, A., Losenno, C., and Pagano, A., 2001, "Experimental Analysis of Thermo-Acoustic Combustion Instability," Applied Energy, 70(2), pp. 179-191.

[5] Rayleigh, J., 1878, "The Explanation of Certain Acoustical Phenomena," eds., London, 3, pp. 536-542.

[6] Anderson, K. R., Hertzberg, J., and Mahalingam, S., 1996, "Classification of Absolute and Convective Instabilities in Premixed Body Stabilized Flames," Combustion Science and Technology, 112(1), pp. 257-269.

[7] Wicksall, D. M., and Agrawal, A. K., 2007, "Acoustics Measurements in a Lean Premixed Combustor Operated on Hydrogen/Hydrocarbon Fuel Mixtures," International Journal of Hydrogen Energy, 32(8), pp. 1103-1112.

[8] Chan, C. K., Lau, K. S., Chin, W. K., and Cheng, R. K., 1992, "Freely Propagating Open Premixed Turbulent Flames Stabilized by Swirl," Proceedings of the Combustion Institute, 24(1-2), pp. 511-518.

[9] Cheng, R. K., Yegian, D. T., Miyasato, M. M., Samuelsen, G. S., Pellizzari, R., Loftus, P., and Benson, C., 2000, "Scaling and Development of Low-Swirl Burners for Low-Emission Furnaces and Boilers," Proceedings of the Combustion Institute, 28(1), pp. 1305-1313.

[10] Kortschik, C., Plessing, T., and Peters, N., 2004, "Laser Optical Investigation of Turbulent Transport of Temperature Ahead of the Preheat Zone in a Premixed Flame," Combustion and Flame, 136(1-2), pp. 43-50.

[11] Petersson, P., Olofsson, J., Brackman, C., Seyfried, H., Zetterberg, J., Richter, M., Aldén, M., Linne, M. A., Cheng, R. K., Nauert, A., Geyer, D., and Dreizler, A., 2007, "Simultaneous Piv/Oh-Plif, Rayleigh Thermometry/Oh-Plif and Stereo Piv Measurements in a Low-Swirl Flame," Applied Optics, 46(19), pp. 3928-3936.

[12] Shepherd, I. G., Cheng, R. K., Plessing, T., Kortschik, C., and Peters, N., 2002, "Premixed Flame Front Structure in Intense Turbulence," Proceedings of the Combustion Institute, 29(2), pp. 1833-1840.

[13] Johnson, M. R. A. L., D. And Nazeer, W. A. And Smith, K. O. And Cheng, R. K., 2005, "A Comparison of the Flowfields and Emissions of High-Swirl Injectors and Low-Swirl Injectors for Lean Premixed Gas Turbines," Proceedings of the Combustion Institute, 30(2), pp. 8.

[14] Cheng, R. K., Fable, S. A., Schmidt, D., Arellano, L., and Smith, K. O., 2001, "Development of a Low Swirl Injector Concept for Gas Turbines," 2001 International Joint Power Conference.

[15] Littlejohn, D., and Cheng, R. K., 2007, "Fuel Effects on a Low-Swirl Injector for Lean Premixed Gas Turbines," Proceedings of the Combustion Institute, 31(2), pp. 8.

[16] Cheng, R. K., Littlejohn, D., Strakey, P. A., and Sidwell, T., 2009, "Laboratory Investigations of a Low-Swirl Injector with H2 and Ch4 at Gas Turbine Conditions," Proceedings of the Combustion Institute, 32, pp. 8.

[17] Kang, D. M., Culick, F. E. C., and Ratner, A., 2007, "Combustion Dynamics of a Low-Swirl Combustor," Combustion and Flame, 151(3), pp. 412-425.

[18] Wernet, M. P., 1999, "Fuzzy Logic Enhanced Digital Piv Processing Software," 18th International Congress on Instrumentation in Aerospace Simulation Facilities.

[19] Portillo, J. E., Sisco, J. C., Yu, Y. C., Sankaran, V., and Anderson, W. E., 2007, "Application of a Generalized Instability Model to a Longitudinal Mode Combustion Instability," 43rd AIAA/ASME/SAE/ASEE Joint Propulson Conference and Exhibition, AIAA Paper 2007-5651.

[20] Yu, Y. C., Sisco, J. C., Merkle, C. L., Anderson, W. E., and Sankaran, V., 2007, "The Examination of Spatial Mode Shapes and Resonant Frequencies Using Linearized Euler Solutions," eds., Miami, FL, AIAA Paper 2007-3993.

[21] Culick, F. E. C., 1989, "Combustion Instabilities in Liquid-Fueled Propulsion Systems - an Overview," eds., CP-450, pp.

[22] Smith, R. J., 2006, "Computational Modeling of High Frequency Combustion Instability in a Single-Element Liquid Rocket," Ph.D. thesis, Purdue University, West Lafayette.